

## Article

# Experimental Investigations of Flow Boiling Heat Transfer under Near-Critical Pressure for Selected Working Fluids

Dariusz Butrymowicz <sup>1,\*</sup> , Kamil Śmierciew <sup>1</sup> , Jarosław Karwacki <sup>2</sup> , Aleksandra Borsukiewicz <sup>3</sup>   
and Jerzy Gagan <sup>1</sup> 

<sup>1</sup> Department of Thermal Engineering, Białystok University of Technology, 15-351 Białystok, Poland

<sup>2</sup> The Szewalski Institute of Fluid-Flow Machinery of Polish Academy of Sciences, 80-231 Gdansk, Poland

<sup>3</sup> Department of Energy Technologies, West Pomeranian University of Technology, 70-310 Szczecin, Poland

\* Correspondence: d.butrymowicz@pb.edu.pl

**Abstract:** This paper deals with experimental investigations of flow boiling in tubular ducts of selected refrigerants—R134a, R507A, and R600a—under near-critical pressures. Near-critical boiling is characterised by low specific enthalpy of evaporation. The positive effect of this feature is the fact that only a small amount of heat consumed by Organic Rankine Cycles is at a constant temperature. This allows a lower terminal temperature of the heating fluid and more effective utilisation of heat sources, especially of low-grade heat sources. The experimental investigations covered a heat flux density of 0.4 to 10 kW/m<sup>2</sup> and a mass velocity of 60 to 200 kg/(m<sup>2</sup>·s). The results of the experimental data were compared to the modified heat transfer correlation of Gungor and Winterton, which provides the best fit for the obtained experimental data. The maximum heat transfer coefficient occurred at the two-phase quality—approximately 0.4 for all the tested fluids under high pressure conditions—which may be thought of as a characteristic feature of the boiling process under near-critical conditions. A modified Gungor–Winterton correlation improves prediction accuracy, especially under the lowest (up to 3 kW/m<sup>2</sup>) and highest (over 7 kW/m<sup>2</sup>) heat flux densities for all the tested fluids.

**Keywords:** mini-channel heat exchangers; condensers; evaporators; heat transfer; pressure drop; propane



**Citation:** Butrymowicz, D.; Śmierciew, K.; Karwacki, J.; Borsukiewicz, A.; Gagan, J. Experimental Investigations of Flow Boiling Heat Transfer under Near-Critical Pressure for Selected Working Fluids. *Sustainability* **2022**, *14*, 14029. <https://doi.org/10.3390/su142114029>

Academic Editor: Chi-Ming Lai

Received: 8 September 2022

Accepted: 24 October 2022

Published: 28 October 2022

**Publisher's Note:** MDPI stays neutral with regard to jurisdictional claims in published maps and institutional affiliations.



**Copyright:** © 2022 by the authors. Licensee MDPI, Basel, Switzerland. This article is an open access article distributed under the terms and conditions of the Creative Commons Attribution (CC BY) license (<https://creativecommons.org/licenses/by/4.0/>).

## 1. Introduction

Organic Rankine Cycles (ORC) enable cost-efficient power generation from low-grade heat sources by replacing water with organic working fluids, such as various synthetic refrigerants or natural fluids, e.g., hydrocarbons. ORC systems use low-grade heat from various sources such as biomass, geothermal water, and solar and waste heat of industrial processes. ORC is also regarded as a very suitable method to recover the waste heat of internal combustion engines [1–3]. The main differences between the ORC and the conventional Rankine cycle are the working fluid and operating pressures and temperatures. Therefore, the operating performance of an ORC system depends mostly on the properties of the working fluid. However, design and operating characteristics of the cycle are also important. A suitable fluid for an ORC system should have favourable physical, environmental, safety, and economic properties. It is also desirable that working fluid circulating in the ORC system should consume as much heat as possible, which requires a large temperature drop. This can be accomplished by means of a configuration of the system whereby the working fluid is heated using a minimum ratio of latent heat during the evaporation process, i.e., the latent heat should be minimised as much as possible. These conditions are possible in the vicinity of the critical point, as shown in Figure 1.

Numerous works have addressed the selection of ORC fluids based on fluid- and process-related properties by testing various available fluids in ORC simulation models [4–6]. Mikielwicz [7] proposed a simplified thermodynamic criterion for selection of

working fluids and theoretically compared the performances of a few fluids applied in ORC systems for recovering waste heat generated by internal combustion engines. The thermodynamic and thermokinetic properties of the working fluid are among the most important issues in the selection of ORC system working fluid.

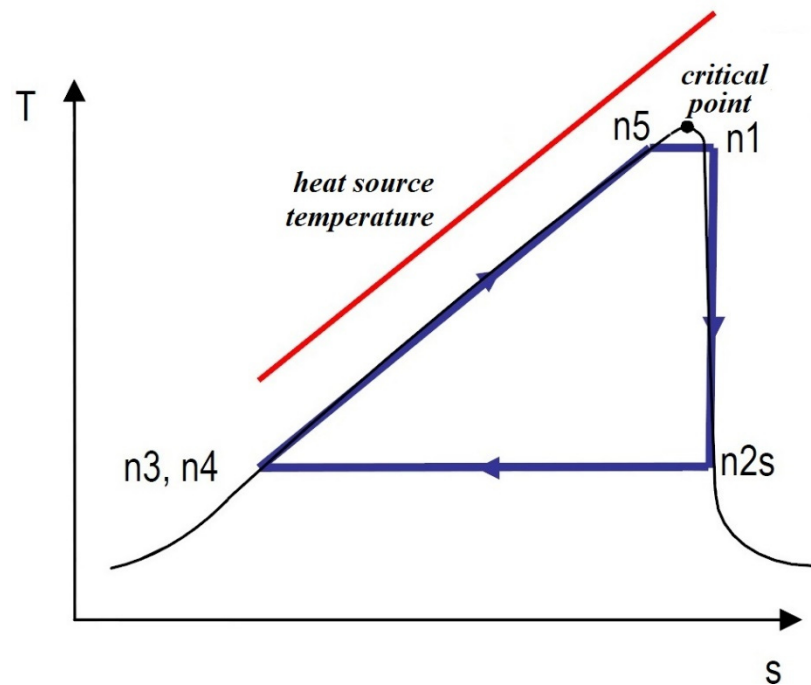


**Figure 1.** The most advantageous shape of the ORC cycle ensuring maximum available heat source thermal capacity (n1—outlet of the vapour generator; n2—turbine outlet; n3, n4—outlet of the condenser and approximate inlet to the vapour generator; n5—boiling process inception).

In most cases, these working fluids are also commonly applied in refrigeration, air-conditioning, and heat-pump technologies. However, thermodynamic properties, and especially thermokinetic properties, change substantially, even with insignificant changes of pressure or temperature at the near-critical point. The latent heat of evaporation and liquid density at the near-critical point decrease more quickly than in lower-pressure areas, resulting in unique boiling heat transfer behaviour. The surface tension and density difference between saturated liquid and the vapour phase gradually decrease with an increase in saturation pressure, and the bubbles' diameters become smaller under high pressure conditions as a result. The generated bubbles are reduced and easily fractured. Meanwhile, the vapour density becomes heavier, potentially leading to assembled vapour blocks [8].

The phenomenon of a boiling crisis and a change of the mode of the boiling process can therefore occur even at near-critical pressure. The boiling process ceases when the pressure is higher than the critical pressure. Observations of the flow under supercritical conditions showed that the heat transfer process is influenced by analogue mechanisms to those occurring in the boiling process (under sub-critical pressure) [9–12]. Numerous studies have been conducted on boiling heat transfer for carbon dioxide during flow in channels and mini-channels [13–15]. However, it should be taken into account that the thermodynamic and thermokinetic properties of carbon dioxide differ significantly from those of many typical synthetic working fluids (belonging to the HFC group), as well as natural fluids (such as hydrocarbons). Let et al. [8] defined the near-critical region as a lower limit pressure equal to  $0.85 p_{cr}$  up to the critical point. Experimental investigations on heat transfer characteristics at supercritical and near-critical pressures are presented by Xu et al. [16]. They applied hexamethyldisiloxane (MM) as a working fluid because

of its low critical parameters, which make it suitable for the medium/high temperature supercritical ORC systems. They have emphasised that under near-critical temperature, the heat exchanger design is one of the most challenging aspects related to the ORC modelling.

Due to changes in fluid properties at the near-critical point, the heat transfer coefficient during evaporation can be overestimated or underestimated [10,17], which is motivation for further studies on boiling heat transfer under high pressure conditions. Modelling of heat transfer in a direct contact evaporator applied to low-grade heat recovery for the ORC system has been investigated by Huang et al. [18]. For heat transfer prediction in the direct contact evaporator, the authors have proposed a method which combines multi-input radial basis function, neural network, and empirical mode decomposition. Direct contact evaporation in micro-scale ORC was also investigated by Pereira et al. [19]. These authors have studied the potential risk of the thermal degradation of the organic fluid, which results from the fact that the combustion gas temperature is well above that of the organic fluid thermal degradation-limiting temperature. Results of near-critical point heat transfer in microchannels while using CO<sub>2</sub> as a working fluid have been presented by Jajja et al. [20]. Infrared thermography has been applied to obtain local heat transfer data. These authors have pointed out that existing supercritical heat transfer correlations developed for uniform wall heating conditions cannot accurately predict heat transfer for single wall heating boundary conditions. Correlations for nucleate pool boiling heat transfer for synthetic refrigerants R245fa and R1233zd (E) applied to the ORC cycle have been proposed by Welzl et al. [21]. Their experimental results have revealed that the heat transfer correlation developed by Cooper as well as the correlation proposed by Gorenflo et al. [22] may be the most accurate with mean absolute deviations between 4.75% and 15.65% for both tested working fluids. Dalkilic et al. [23] proposed empirical correlations for the convective heat transfer in the evaporators for refrigerant R134a. Recently, Belyaev et al. [24] conducted experiments for refrigerants R113 and RC318 in the temperature range from 30 to 180 °C in channels with a diameter of 1.36 mm to 0.95 mm. They noticed that for such high pressures, despite the very small diameter of the channel, the obtained trends resembled those that are characteristic of conventional channels. Extensive research for high pressure conditions was carried out recently by Jakubowska and Mikielewicz [25] on the basis of the previously developed heat transfer correlation of Mikielewicz [26]. They confirmed reasonably good predictivity of the proposed heat transfer correlation for tested fluids. Guo et al. [27] indicated on the basis of systematic experimental research that for R134a in the pressure to critical pressure ratio range from 0.1 to 0.88, convection boiling was the main heat transfer mechanism.

It should also be taken into account that numerous flow boiling heat transfer correlations have been proposed for low and medium saturation pressures, which may be used as a basis for the prediction of heat transfer for high saturation pressure conditions [28,29]. However, there is still a clear need to analyse the applicability of these heat transfer correlations under near-critical conditions, especially for natural working fluids as the most perspective working substances. The above motivates the present experimental investigations of flow boiling in a tubular channel under near-critical pressure. The heat transfer coefficient measurement methodology based on the application of the indirect technique is presented. The primary motivation of the present research is to provide experimental data for isobutane (R 600a) as a natural working substance. Experimental results for near-critical pressures for isobutane in the context of applicability of existing well-known boiling heat transfer correlations may be the main contribution to the state of the art. In order to identify the applicability of heat transfer correlations under near-critical conditions and for other fluids, two synthetic refrigerants, R-134a and R-507A, have been selected as working fluids for the investigations. Therefore, the proposed modification of the boiling heat transfer correlation is based on enlarged experimental data.

## 2. Apparatus and Methodology

### 2.1. Experimental Apparatus

The test facilities were designed and built specially for the purpose of these investigations. The testing loop was modified and instrumented for the refrigerants used as test fluids in order to perform experiments under conditions of high operating pressures. The schematics of the experimental apparatus with the tested heat exchanger applied are shown in Figure 2, and the main components of the stand are listed in the figure description.

The system consists of three loops: refrigerant loop, liquid cooling loop, and liquid heating loop. The test heat transfer section consisted of six tube-in-tube type exchangers, length 528 mm, connected in a series as shown in Figure 2. Detailed geometry of the test section is presented in Figure 3. A photo of the entire test section is presented in Figure 4.

Each of the tube-in-tube heat exchangers was equipped with pressure and temperature sensors. The test section was made of copper. The liquid refrigerant undergoes a boiling process in the inner tube while the heated thermal oil (propylene glycol) flows through the annulus. The diameter of the inner tube is 12.0 mm, the diameter of the outside tube is 22.0 mm, and the thickness of both the inner and outer tube walls is 1.0 mm. In the heating liquid loop, electric heaters of 20 kW and 40 kW were used. The condenser cooling system was equipped with an automatically controlled fan cooler. In both loops, propylene glycol was used as the working fluid. Additionally, both loops are equipped with liquid pumps supplied with frequency converters. This allows the adjustment of the refrigerant flow rates, as well as for varying of thermal parameters in a wide range. Both systems are fully instrumented with transducers for measurement of temperatures, pressures, and flow rates. The design of the entire testing rig allows the precise maintenance of all test parameters within a specific range. The test-stand was equipped with temperature sensors and pressure transducers installed in the critical locations and other locations of interest. Additionally, sight-glasses were installed at various locations to observe the flow pattern. For all data acquisition, a modular system with low-noise chassis and dedicated amplifiers connected to a high-speed multifunction data acquisition module installed in the PC was used. The computer uses dedicated data acquisition and data processing software that can receive on-line data from the NIST database [30].

The testing stand was equipped with a high-class calibration system for measurement paths, pressure and temperature transducers, and flow meters. All sensors and transducers have been calibrated in accordance with ISO 9000. The calibration of thermocouples used on the tested exchanger is made before each measurement series with an accuracy of  $\pm 0.15$  K within the range provided for in the tests. Mutual deviations of thermocouples are not greater than  $\pm 0.1$  K. For the measurements of mass flow rate of glycol and boiling fluid, Endress-Hauser Promass 83 mass flow meters with measurement accuracy of 0.1% for the liquid phase were used. Two kinds of pressure transducers were applied in the testing stand, i.e., Endress + Hauser Cerabar S PMC71 (maximum pressure 40 bar located at the outlet of the liquid pump (see point 2, Figure 2), and the rest were Druck pressure transducers (maximum pressure 40 bar). The DPI-145 calibrator was used to calibrate the pressure measurement path. Taking into account the measurement ranges of the pressure sensors, the calibration was carried out in the pressure range of  $3 \div 20$  bar. During the pressure transducer calibration procedure, after checking the tightness of the system, it was pressurized with nitrogen to an absolute pressure of about 20 bar. The readings of the DPI-145 calibrator were considered as the basis for the calibration procedure. The measurement system recorded the indications of individual transducers. During the measurements, at least 100 samples were taken for each recorded pressure, from which the average value was determined. Reference pressure indications were recorded manually. In the proper tests, the pressure measurement paths will be recalibrated for the values provided in the boiling tests in the near-critical range for the selected working medium. The average accuracy of pressure measurement was  $\pm 0.3\%$  of the transducer readings for the entire pressure measurement path. On the basis of the above presented measurement uncertainties, the

average measurement error of the heat flux calculated by the total differential method for the test sections for the entire measurement range was approx. 12%.

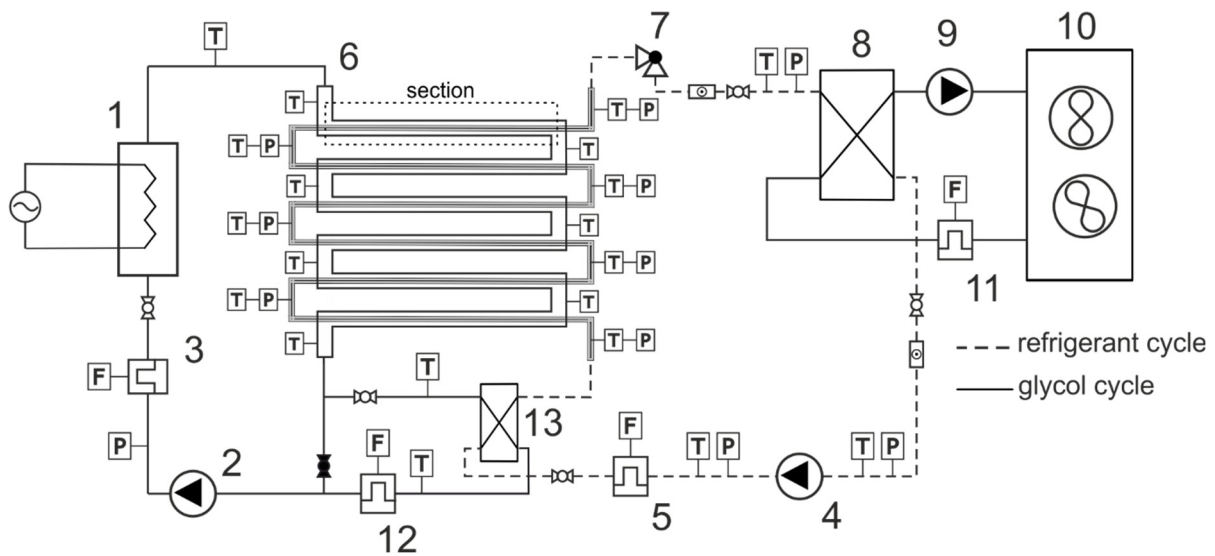


**Figure 2.** Schematic of the experimental stand: 1—electric heater, 2,9—glycol circulation pump, 3,5,11—mass flow meter, 4—refrigerant circulation pump, 6—test heat transfer section, 7—control valve, 8—condenser, 10—fan cooler, 13—auxiliary heat exchanger.

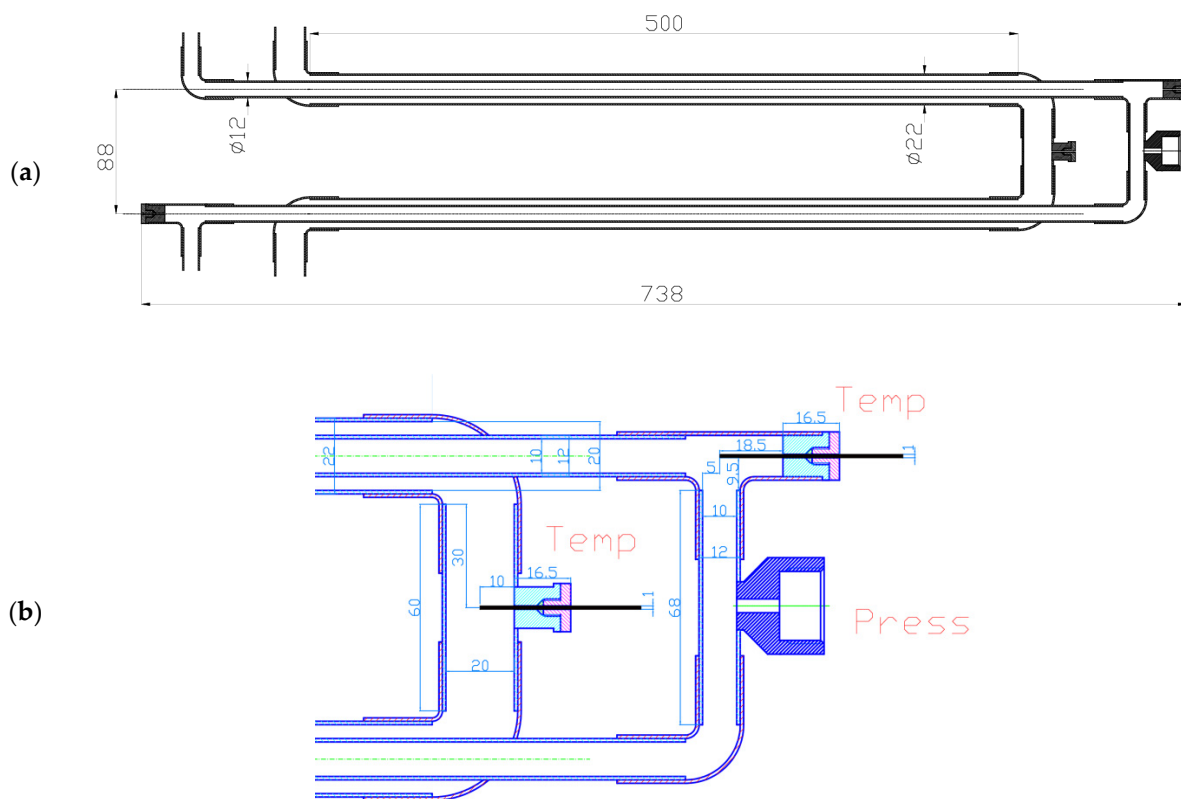


**Figure 3.** Schematic of two heat transfer test sections: (a) dimensions of the sections; (b) details of location of temperature and pressure gauges.



**Figure 4.** Photo of the testing stand.

## 2.2. Methodology of Measurement of Heat Transfer Coefficient

The surface heat transfer coefficient for flow boiling inside tubes in the heat exchanger section was determined by means of separation of the heat transfer resistances. The boiling surface heat transfer coefficient was determined on the basis of the overall heat transfer coefficient  $k$  measurement and measurement of the convective surface heat transfer coefficient for the heating fluid (glycol) side. The overall thermal resistance is:

$$\frac{1}{k} = \frac{1}{\alpha_i} + R_t + \frac{1}{\alpha_o}, \quad (1)$$

where  $k$  is the overall heat transfer coefficient,  $\alpha_i$ ,  $\alpha_o$  are the surface heat transfer coefficients for boiling liquid inside the tube and heating fluid (glycol) in the annulus, respectively, and  $R_t$  is the thermal conductivity resistance of the tube material. Heat flux transferred from the heating glycol to the boiling fluid was calculated as follows:

$$\dot{Q}_g = \dot{m}_g c_g (t_{go} - t_{gi}), \quad (2)$$

where  $\dot{m}_g$  is the mass flow rate of glycol,  $c_g$  is the average specific heat of glycol, and  $t_{gi}$ ,  $t_{go}$  are the glycol temperatures at the heat exchanger inlet and outlet, respectively. All these quantities were measured directly. The overall heat transfer coefficient  $k$  was calculated from the following formula:

$$k = \frac{\dot{Q}_g}{A_w \cdot \Delta T_m}, \quad (3)$$

where  $\Delta T_m$  is the logarithmic difference of temperatures between boiling fluid and heating glycol at the heat exchanger inlets and outlets, and  $A_w$  is the heat transfer surface area. The average temperature of the boiling liquid was calculated as the saturation temperature corresponding to the measured average static pressure inside the test heat exchanger section.

Since the surface heat transfer coefficients for both sides of the tube wall are not known, it is necessary to apply the method based on the thermal resistance separation. In order to determine the surface heat transfer coefficient for the boiling fluid, it is necessary to apply the measurement approach for the surface heat transfer coefficient for the heating fluid side.

The indirect measurement method based on the Wilson plot technique for surface heat transfer coefficient  $\alpha_o$  for heating fluid (glycol) was applied. In this method, no direct measurement of the tube wall temperature (inside or outside of the tube) is required. The wall temperature should be determined on the basis of simultaneous determination of the heat transfer coefficient. The average wall temperature on the glycol side was estimated as follows:

$$t_{wo} = t_{gm} - \frac{\dot{Q}_g}{0.023 A_{wo} \Psi_{go}}, \quad (4)$$

where  $t_{gm}$  is the logarithmic average glycol temperature in the test heat exchanger section, and for the turbulent and transient flow the coefficient  $\Psi_{go}$  is defined with the use of the Sieder and Tate [31] heat transfer correlation as follows:

$$\Psi_{go} = \frac{\lambda_g}{D_{gc}} \cdot \text{Re}_g^{0.80} \cdot \text{Pr}_g^{0.40}, \quad (5)$$

where  $D_{gc}$  denotes the hydraulic diameter of the annulus for glycol flow. The heat transfer coefficient for glycol  $\alpha_o$  was therefore determined using the following formula:

$$\alpha_o = C_o \cdot \Psi_o, \quad (6)$$

Additionally,

$$\Psi_o = \Psi_{go} \left( \frac{\mu_g(t_{gm})}{\mu_g(t_{wo})} \right)^{0.14} \quad (7)$$

The coefficient  $C_o$  is the first unknown constant parameter that should be obtained on the basis of the experimental data. Analogically, the average wall temperature at the evaporating liquid side inside the tube was estimated from the following equation:

$$t_{wi} = t_{rm} + \frac{\dot{Q}_g}{0.023 A_{wi} \Psi_{ri}}, \quad (8)$$

where  $t_{rm}$  is the logarithmic average refrigerant temperature in the test heat exchanger section (assumed as average saturation temperature on the basis of the measurement of static pressure at the inlet and outlet of the test section). The coefficient  $\Psi_{ri,t}$  is defined assuming the turbulent and transient flow of one-phase fluid with the application of the Sieder and Tate heat transfer correlation [8]:

$$\Psi_{ri,t} = \frac{\lambda_{rl}}{D_i} \text{Re}_r^{0.80} \text{Pr}_r^{0.40} \quad (9)$$

In the case of laminar flow inside the test tube section, the well-known heat transfer correlation for laminar flow proposed by Sieder and Tate [31] was applied:

$$Nu_i = \frac{\alpha_i D_i}{\lambda_r} = 0.015 \left( \text{Re}_r \text{Pr}_r \frac{D_i}{L} \right)^{0.33} \quad (10)$$

Therefore, for laminar flow, the following coefficient was applied:

$$\Psi_{ri,l} = \frac{\lambda_r}{D_i} \left( \text{Re}_r \text{Pr}_r \frac{D_i}{L} \right)^{0.33} \quad (11)$$

The surface heat transfer coefficient for inside the tube wall  $\alpha_i$  is:

$$\alpha_i = C_i \Psi_i, \quad (12)$$

Furthermore:

$$\Psi_i = \Psi_{ri} \left( \frac{\mu_r(t_{rm})}{\mu_r(t_{wi})} \right)^{0.14}, \quad (13)$$

where  $\Psi_{ri} = \Psi_{ri,t}$  for turbulent flow, and  $\Psi_{ri} = \Psi_{ri,l}$  for laminar flow.

Note that in this case it is necessary to carry out the dedicated measurements with a single-phase flow of refrigerant inside the tube. This part of the experimental investigations may be viewed as a calibration test due to the way that the heat transfer coefficient for the heating fluid side (glycol) should be identified. The discussed calibration measurements were carried out using liquid subcooled refrigerant R134a.

Based on the above considerations, Equation (1) can be transformed into the following form:

$$\left( \frac{1}{k} - R_t \right) \cdot \Psi_o \cdot \frac{A_{wo}}{A_{wi}} = C_i^{-1} \cdot \frac{\Psi_o}{\Psi_i} \cdot \frac{A_{wo}}{A_{wi}} + C_o^{-1} \quad (14)$$

The thermal resistance of the tube was calculated as:

$$R_t = \frac{\delta_t D_i}{\lambda_t D_m} \quad (15)$$

Using linear regression, the parameters  $C_i$  and  $C_o$  can be calculated. Assuming the following notation:

$$Y = \left( \frac{1}{k_i} - R_t \right) \Psi_o \frac{A_{wo}}{A_{wi}}, \quad (16)$$

and

$$X = \frac{\Psi_o}{\Psi_i} \cdot \frac{A_{wo}}{A_{wi}}, \quad (17)$$

The following linear relationship is obtained:

$$Y = C_o^{-1} + C_i^{-1} X \quad (18)$$

The constants  $C_o$  and  $C_i$  were determined on the basis of the reference measurements with a single-phase flow of subcooled liquid refrigerant R-134a inside the tube, and heated glycol flow in the annulus. These constants were determined by means of linear regression. In these experiments, the obtained coefficient  $C_o$  was applied for calculations of the surface heat transfer coefficient for the glycol side.

The main parts of the experimental investigations were carried out for the conditions of the boiling process inside the tube. Having the coefficient  $C_o$  for glycol flowing in the annulus, it is possible to apply Equations (6) and (7) for calculation of the surface heat transfer coefficient  $\alpha_o$  for glycol. The surface heat transfer coefficient for boiling refrigerant inside the tube was calculated from Equation (1).

### 2.3. Calibration Results of Heat Transfer for Heating Fluid Side

Since the modified Wilson plot technique was used in calculation, the results of the linear regression are shown in Figure 5, in which coordinates  $Y$  and  $X$  were calculated using Equations (15) and (16), respectively.

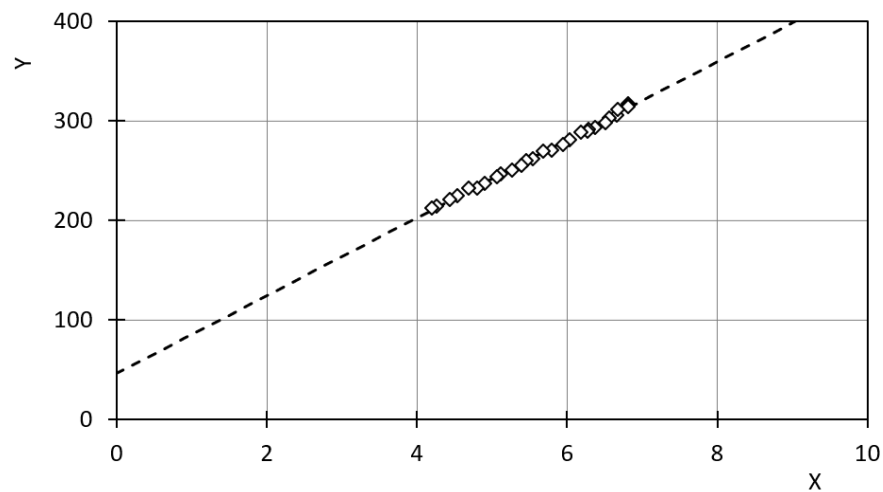


**Figure 5.** Experimental results of linear regression for calculation of parameters  $C_o$  by means of modified Wilson plot technique for turbulent flow of heating glycol.

In Table 1, the coefficients  $C_o$  and  $C_i$  obtained from experimental data are shown. Note that in the original heat transfer correlation for turbulent flow [8] the constant is 0.023, and for the case of laminar flow the constant is 0.015. However, these original constants may be applied for hydraulically and thermally developed flow. The obtained results indicate that such conditions did not occur in the testing stand, which was motivation for the testing stand calibration that ensures improved accuracy of the obtained experimental data. The constant coefficient  $C_o$  is the basis for calculation of the glycol side surface heat transfer coefficient  $\alpha_o$ .

**Table 1.** The coefficients  $C_o$  and  $C_i$  obtained from the reference measurements.

Heating Glycol Flow	Coefficient	Value
laminar	$C_o/0.015$	0.93133
turbulent	$C_o/0.023$	1.16479

### 3. Experimental Results

The experimental investigations covered the measurement of the average heat transfer coefficient for isobutane (R600a) and two synthetic fluids, R-134a and R-507A, under conditions of various levels of pressure at the inlet to the tested heat transfer sections. The experiment ran heat flux density 0.6 to 10 kW/m<sup>2</sup> and mass velocity 60 to 200 kg/(m<sup>2</sup>·s). The measurement approach presented in Section 2.2 was applied for each tube-in-tube heat transfer section. Therefore, the obtained results may be thought as a kind of local surface heat transfer coefficient. Local two-phase quality of the two-phase flow was determined on the basis of the energy balance of each tested heat transfer section of the tubular heat exchanger. The test conditions are presented in Table 2. The selected results of the single series for each type of investigated refrigerant are presented in Figures 6–8.

**Table 2.** Parameters of the experimental investigations of boiling heat transfer.

Working Fluid	$p/p_{cr}$	$q$ [kW/m <sup>2</sup> ]	$G$ [kg/(m <sup>2</sup> ·s)]
R600a	0.501–0.893	0.39–10.42	28.01–67.68
R134a	0.700–0.856	0.43–9.94	54.43–190.0
R507A	0.503–0.985	0.34–5.35	56.09–126.3

The maximum heat transfer coefficient was obtained for the investigated cases at the two-phase quality—approximately 0.4—while for significantly lower pressure the

maximum heat transfer coefficient for flow boiling is observed at the local quality of app. 0.7–0.8. The heat transfer coefficient for the quality of two-phase flows higher than 0.4 scarcely depends on the quality. The observed effect of a shift of quality at which there is observed maximum heat transfer to a significantly lower level may be explained as a result of the change in the thermokinetic properties under near-critical conditions. The surface tension and density difference between saturated liquid and vapour decreases with an increase in saturation pressure. Therefore, the bubble diameters become smaller under high pressure conditions, which is the reason for the shifting of the mist-annular two-phase pattern flow to a lower level of two-phase quality.

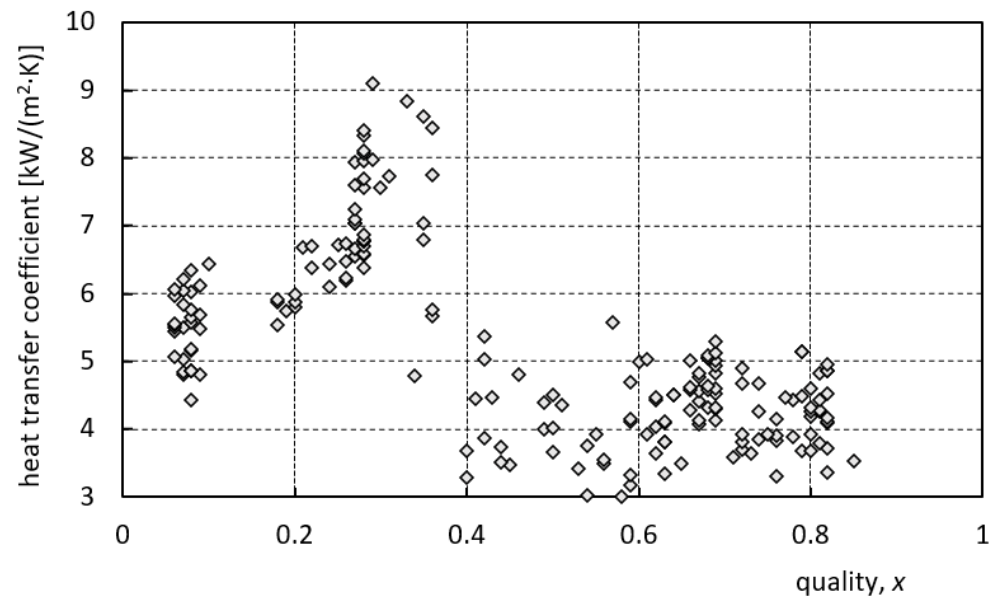


**Figure 6.** Surface heat transfer coefficient  $\alpha_i$  vs. local quality for refrigerant R134a, pressure ratio  $p/p_{cr} = 0.84$  for various mass flow rates.

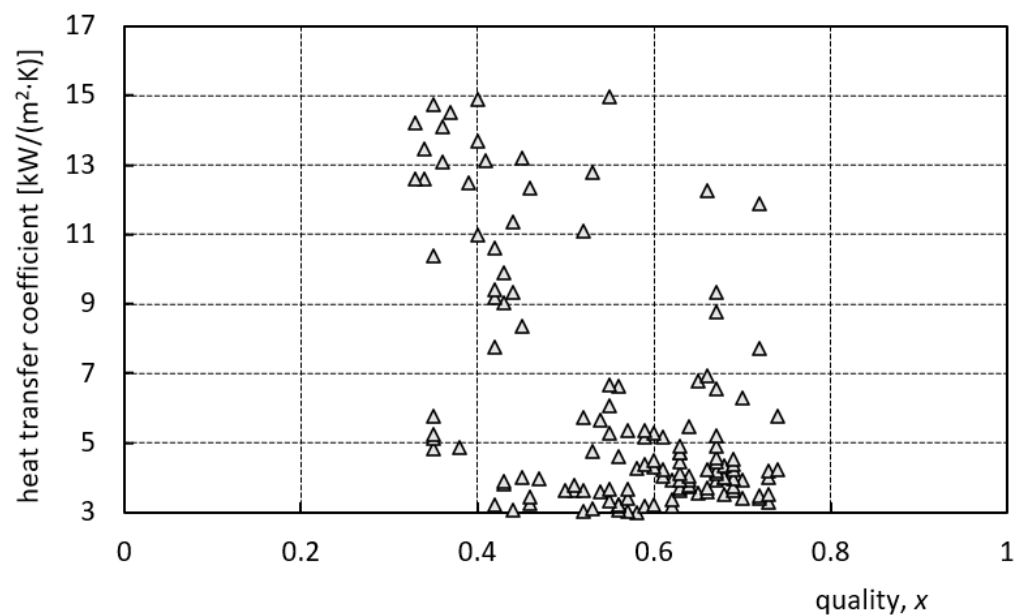


**Figure 7.** Surface heat transfer coefficient  $\alpha_i$  vs. local quality for refrigerant R507A, pressure ratio  $p/p_{cr} = 0.83$  for various mass flow rates.

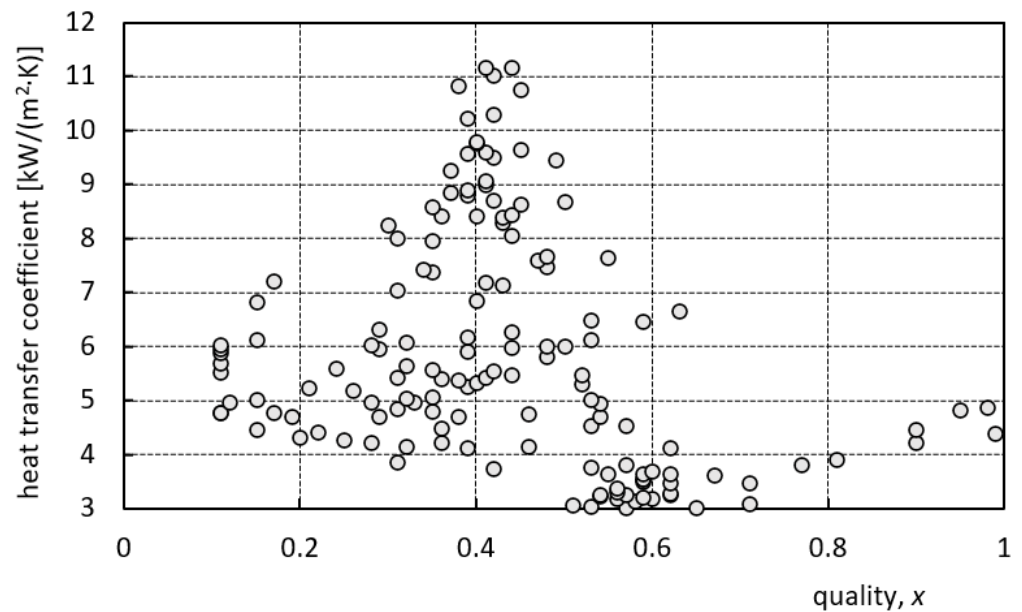


**Figure 8.** Heat transfer coefficient  $\alpha_i$  vs. local quality for isobutane R600a, pressure ratio  $p/p_{cr} = 0.72$  for various mass flow rates.

The authors tested several boiling heat transfer correlations provided in the literature [31–33] including correlations proposed by Chen, Steiner and Taborek, both given in [31], Gungor and Winterton [32], and Shah given in [33]. On the basis of these investigations, it may be concluded that the correlation of Gungor–Winterton gives the best fit values of the heat transfer coefficient. Gungor and Winterton proposed the following relationship [32]:

$$\alpha_{GW} = \alpha_{conv}E + \alpha_{pb}S \quad (19)$$

The quantities applied in Equation (19) are as follows—convective heat transfer coefficient for turbulent flow:

$$\alpha_{conv} = 0.023 \frac{\lambda}{D_i} \text{Re}_l^{0.80} \text{Pr}^{0.40}, \quad (20)$$

The pool boiling heat transfer coefficient according to the heat transfer correlation proposed by Cooper [34] is:

$$\alpha_{pb} = 55 p_R^{0.12} (-\log p_R)^{-0.55} M^{-0.50} q^{0.67}, \quad (21)$$

where  $p_R$  is reduced pressure  $p/p_{cr}$ ,  $M$ —molar mass, and  $q$ —heat flux density. The two-phase convection multiplier  $E$  is equal to:

$$E = 1 + 24000 B_o^{1.16} + 1.37 \chi^{-0.86}, \quad (22)$$

where the Lockhart–Martinelli parameter is defined as follows:

$$\chi = \left( \frac{\rho''}{\rho'} \right)^{0.5} \left( \frac{\mu'}{\mu''} \right)^{0.1} \left( \frac{1-x}{x} \right)^{0.9}, \quad (23)$$

The boiling suppression factor  $S$  is given as follows:

$$S = \left[ 1 + 1.15 \cdot 10^{-6} E^2 \text{Re}_{ri}^{1.17} \right]^{-1}. \quad (24)$$

The Boiling number  $Bo$  is defined as follows:

$$Bo = \frac{q}{h_{fg}G(1-x)}. \quad (25)$$

The ratio of the heat transfer coefficient obtained from the above Gungor–Winterton correlation to the experimental values,  $\alpha_{G-W}/\alpha_{exp}$ , is presented in Figure 9.

The original heat transfer correlation proposed by Gungor–Winterton overpredicts the surface heat transfer coefficient for low heat fluxes and underpredicts the heat transfer coefficient in comparison with the experimental data for high heat fluxes (see Figure 9). Therefore, the authors propose the following modification of this correlation elaborated for all tested refrigerants:

$$\alpha_{cor} = \alpha_{GW} \exp[-45.8(1 - Bo_m^{-0.016})], \quad (26)$$

where the modified boiling number is defined as follows:

$$Bo_m = \frac{ql_k \rho'}{h_{fg} \mu' \rho''}, \quad (27)$$

The capillary constant is defined as follows:

$$l_k = \sqrt{\frac{\sigma}{g(\rho' - \rho'')}}. \quad (28)$$

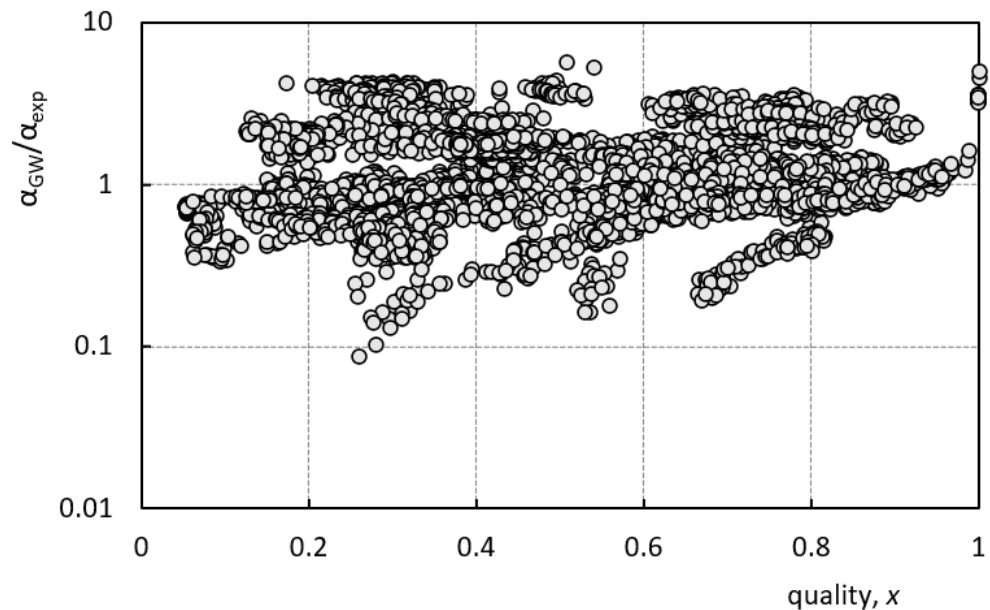


**Figure 9.** Ratio of predicted and measured heat transfer coefficient  $\alpha_{G-W}/\alpha_{exp}$  vs. quality of two-phase flow.

A comparison of the proposed modified heat transfer correlation, Equation (26), with predictions based on the original Gungor–Winterton correlation, Equation (19), and experimental data is presented in Figure 10. The coefficient of determination for the entire experimental data for the proposed heat transfer correlation is  $R^2 = 0.51$ . The proposed correction significantly improves the prediction of the heat transfer coefficient for the lowest and highest heat flux densities.

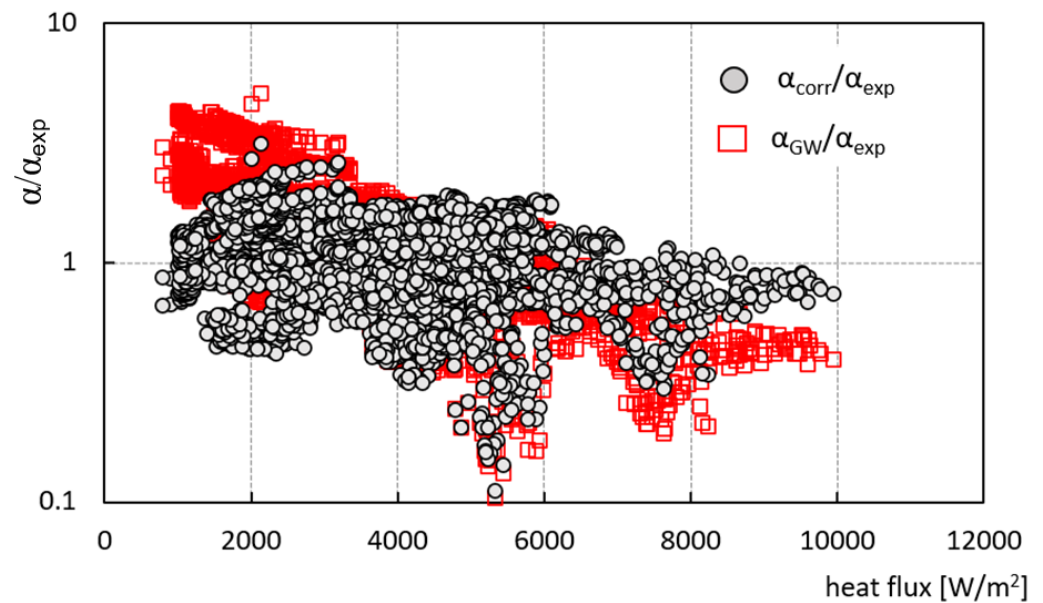


**Figure 10.** Comparison of own heat transfer correlation, Equation (26) with correlation of Gungor and Winterton, Equation (19) with experimental data of heat transfer coefficient vs. heat flux density  $q$  for various mass flow rates and two-phase qualities.

#### 4. Conclusions

The measurement procedure for the local heat transfer coefficient for flow boiling of selected working fluids dedicated to the ORC cycle was presented. Heat transfer coefficients were determined by means of separation of the thermal resistances. The calibration procedure of the tested heat exchanger with the measurement sections by means of the modified Wilson plot technique was applied. The selected experimental results of the surface heat transfer coefficient are presented for three tested fluids, i.e., isobutane (R600a) as a natural working fluid and two synthetic fluids, R-134a and R-507A. The experimental investigations covered a heat flux density of 0.6 to 12 kW/m<sup>2</sup> and a mass velocity of 60 to 200 kg/(m<sup>2</sup>·s). The following conclusions may be drawn on the basis of the obtained experimental results:

- The maximum heat transfer coefficient occurred for the two-phase quality of approximately 0.4 for all the tested fluids under high pressure conditions. Note that the two-phase quality at which there is a maximum heat transfer coefficient under low and moderate pressures is app. 0.7–0.8. A shift of quality of the maximum heat transfer coefficient may be viewed as a result of thermokinetic property changes under near-critical pressure conditions. The above may be thought of as a characteristic feature of the boiling process under near-critical conditions.
- The Gungor–Winterton boiling heat transfer correlation may be recommended for application to tested fluids. However, this heat transfer correlation overpredicts surface heat transfer coefficients for lowest (up to 3 kW/m<sup>2</sup>) and highest (over 7 kW/m<sup>2</sup>) heat flux densities for all tested fluids.
- In order to improve the accuracy of the Gungor–Winterton heat transfer correlation, its modification was proposed based on a multiplier with a modified Boiling number. The coefficient of determination for the entire experimental data for the proposed modified heat transfer correlation is  $R^2 = 0.51$ .

There is still a clear need to continue this research on boiling heat transfer, especially in the close vicinity of the critical point, and especially for natural substances as a prospective working fluid for power engineering systems.

**Author Contributions:** Conceptualization, A.B.; Data curation, K.Ś. and J.G.; Investigation, J.K.; Methodology, D.B. All authors have read and agreed to the published version of the manuscript.

**Funding:** This work was conducted with the support of research funds under the statutory work WZ/WM-IIM/1/2020 carried out at the Institute of Mechanical Engineering of the Bialystok University of Technology.

**Institutional Review Board Statement:** Not applicable.

**Informed Consent Statement:** Not applicable.

**Data Availability Statement:** Not applicable.

**Conflicts of Interest:** The authors declare no conflict of interest.

## Nomenclature

$A$	surface area, $m^2$
$Bo$	boiling number, Equation (27)
$C$	constant of Wilson plot technique
$c$	specific heat at constant pressure, $J/(kg \cdot K)$
$D$	diameter, $m$
$E$	convection multiplier, Equation (22)
$G$	mass velocity, $kg/(m^2 \cdot s)$
$g$	gravitational acceleration, $m/s^2$
$h$	specific enthalpy, $J/kg$
$k$	overall heat transfer coefficient, $W/(m^2 \cdot K)$
$L$	length, $m$
$l$	constant, Equation (27)
$M$	molar mass, $kg/kmol$
$\dot{m}$	mass flow rate, $kg/s$
$Nu$	Nusselt number, $Nu = \alpha D/\lambda$
$Pr$	Prandtl number, $Pr = \mu c/\lambda$
$\dot{Q}$	heat flux, $W$
$q$	heat flux density, $W/m^2$
$R$	thermal resistance, $m^2 \cdot K/W$
$Re$	Reynolds number, $Re = GD/\mu$
$S$	boiling suppression factor, Equation (23)
$t$	temperature, $^{\circ}C$
$X$	reduced Wilson plot technique coordinate
$x$	quality of two-phase flow
$\gamma$	surface tension, $N/m$

## Greek symbols

$\alpha$	surface heat transfer coefficient, $W/(m^2 \cdot K)$
$\chi$	Lockhart-Martinelli parameter, Equation (23)
$\lambda$	thermal conductivity, $W/(m \cdot K)$
$\mu$	dynamic viscosity, $Pa \cdot s$
$\rho$	density, $kg/m^3$
$\sigma$	surface tension, $N/m$

## Subscripts

$bc$	pool boiling
$cr$	critical
$conv$	convection
$fg$	vaporisation
$g$	glycol (heating fluid)
$i$	inside; inlet
$k$	capillary
$l$	laminar flow; liquid phase
$m$	mean; modified

<i>r</i>	refrigerant (boiling fluid)
<i>o</i>	outlet; outside
<i>t</i>	tube; turbulent flow
<i>v</i>	vapour phase
<i>w</i>	tube wall
'	saturated liquid
"	saturated vapour

## References

- Liu, P.; Shu, G.; Tian, H.; Wang, X.; Yu, Z. Alkanes based two-stage expansion with interheating Organic Rankine cycle for multi-waste heat recovery of truck diesel engine. *Energy* **2018**, *147*, 337–350. [\[CrossRef\]](#)
- Shu, G.; Liu, P.; Tian, H.; Wang, X.; Jing, D. Operational profile based thermal-economic analysis on an Organic Rankine cycle using for harvesting marine engine's exhaust waste heat. *Energy Convers. Manag.* **2017**, *146*, 107–123. [\[CrossRef\]](#)
- Mastrullo, R.; Mauro, A.W.; Revellin, R.; Viscito, L. Modeling and optimization of a shell and louvered fin mini-tubes heat exchanger in an ORC powered by an internal combustion engine. *Energy Convers. Manag.* **2015**, *101*, 697–712. [\[CrossRef\]](#)
- Pan, L.; Wang, H.; Shi, W. Performance analysis in near-critical conditions of organic Rankine cycle. *Energy* **2012**, *37*, 281–286. [\[CrossRef\]](#)
- Shu, G.; Wang, X.; Tian, H.; Liu, P.; Jing, D.; Li, X. Scan of working fluids based on dynamic response characters for Organic Rankine Cycle using for engine waste heat recovery. *Energy* **2017**, *133*, 609–620. [\[CrossRef\]](#)
- Papadopoulos, A.I.; Stijepovic, M.; Linke, P. On the systematic design and selection of optimal working fluids for Organic Rankine Cycles. *Appl. Therm. Eng.* **2010**, *30*, 760–769. [\[CrossRef\]](#)
- Mikielewicz, D.; Mikielewicz, J. A thermodynamic criterion for selection of working fluid for subcritical and supercritical domestic micro CHP. *Appl. Therm. Eng.* **2010**, *30*, 2357–2362. [\[CrossRef\]](#)
- Lei, L.; Zhang, W.; Zhang, J.; Dinh, N.; Li, H. Experimental investigations on the boiling heat transfer of horizontal flow in the near-critical region. *Int. J. Heat Mass Transf.* **2018**, *125*, 618–628. [\[CrossRef\]](#)
- Howell, J.R.; Lee, S.H. Convective heat transfer in the entrance region of a vertical tube for water near the thermodynamic critical point. *Int. J. Heat Mass Transf.* **1999**, *42*, 1177–1187. [\[CrossRef\]](#)
- Lee, S.H. Convective heat transfer to water near the critical region in a horizontal square duct. *Int. J. Heat Mass Transf.* **2008**, *51*, 2930–2939. [\[CrossRef\]](#)
- Lee, S.H. Transient convective heat transfer to water near the critical region in a vertical tube. *Int. Commun. Heat Mass Transf.* **2006**, *33*, 610–617. [\[CrossRef\]](#)
- Lee, S.H.; Howell, J.R. Turbulent development convective heat transfer in a tube for fluids near the critical point. *Int. J. Heat Mass Transf.* **1999**, *41*, 1205–1218. [\[CrossRef\]](#)
- Liu, G.; Huang, Y.; Wang, J.; Lv, F.; Leung, L.K.H. Experiments on the basic behavior of supercritical CO<sub>2</sub> natural circulation. *Nucl. Eng. Des.* **2016**, *300*, 376–383. [\[CrossRef\]](#)
- Thome, J.R.; El Hajal, J. Flow boiling heat transfer to carbon dioxide: General prediction method. *Int. J. Refrig.* **2004**, *27*, 294–301. [\[CrossRef\]](#)
- Pan, M.; Chen, X.; Li, X. Multi-objective analysis and optimization of cascade supercritical CO<sub>2</sub> cycle and organic Rankine cycle systems for waste-to-energy power plant. *Appl. Therm. Eng.* **2022**, *214*, 118882. [\[CrossRef\]](#)
- Xu, G.; Fu, J.; Quan, Y.; Wen, J.; Dong, B. Experimental investigation on heat transfer characteristics of hexamethyldisiloxane (MM) at supercritical pressures for medium/high temperature ORC applications. *Int. J. Heat Mass Transf.* **2020**, *156*, 119852. [\[CrossRef\]](#)
- Cheng, L.; Ribatski, G.; Wojtan, L.; Thome, J.R. New flow boiling heat transfer model and flow pattern map for carbon dioxide evaporating inside horizontal tubes. *Int. J. Heat Mass Transf.* **2005**, *49*, 4082–4094. [\[CrossRef\]](#)
- Huang, J.; Xiao, Q.; Liu, J.; Wang, H. Modeling heat transfer properties in an ORC direct contact evaporator using RBF neural network combined with EMD. *Energy* **2019**, *173*, 306–316. [\[CrossRef\]](#)
- Pereira, J.S.; Almeida, J.; Andre, J.C.; Mendes, R.; Ribeiro, J.B. Modelling and experimental validation of the heat-transfer processes of a direct vaporization micro-scale ORC-evaporator for thermal degradation risk assessment. *Energy Convers. Manag.* **2021**, *238*, 114130. [\[CrossRef\]](#)
- Jajja, S.A.; Fronk, B.M. Investigation of near-critical heat transfer in rectangular microchannels with single wall heating using infrared thermography. *Int. J. Heat Mass Transf.* **2021**, *177*, 121470. [\[CrossRef\]](#)
- Welzl, M.; Heberle, F.; Brüggemann, D. Experimental evaluation of nucleate pool boiling heat transfer correlations for R245fa and R1233zd(E) in ORC applications. *Renew. Energy* **2020**, *147 Pt 3*, 2855–2864. [\[CrossRef\]](#)
- Gorenflo, D.; Baumhögger, E.; Herres, G.; Kotthoff, S. Prediction methods for pool boiling heat transfer: A state-of-the-art review. *Int. J. Refrig.* **2014**, *43*, 203–226. [\[CrossRef\]](#)
- Dalkilic, A.S.; Celen, S.; Çebi, A.; Wongwises, S. Empirical correlations for the determination of R134a's convective heat transfer coefficient in horizontal and vertical evaporators having smooth and corrugated tubes. *Int. Commun. Heat Mass Transf.* **2016**, *76*, 85–97. [\[CrossRef\]](#)

24. Belyaev, A.V.; Varava, A.N.; Dedov, A.V.; Komov, A.T. An experimental study of flow boiling in minichannels at high reduced pressure. *Int. J. Heat Mass Transf.* **2017**, *110*, 360–373. [[CrossRef](#)]
25. Jakubowska, B.; Mikielwicz, D. An improved method for flow boiling heat transfer with account of the reduced pressure effect. *Therm. Sci.* **2019**, *23*, 1261–1272. [[CrossRef](#)]
26. Mikielwicz, D. A New Method for Determination of Flow Boiling Heat Transfer Coefficient in Conventional-Diameter Channels and Minichannels. *Heat Transf. Eng.* **2010**, *31*, 276–287. [[CrossRef](#)]
27. Guo, Q.; Li, M.; Tian, X. Experimental study on flow boiling heat transfer characteristics of R134a, R245fa and R134a/R245fa mixture at high saturation temperatures. *Int. J. Therm. Sci.* **2020**, *150*, 106195. [[CrossRef](#)]
28. Ye, Z.; Zendejboudi, A.; Hafner, A.; Cao, F. General heat transfer correlations for supercritical carbon dioxide heated in vertical tubes for upward and downward flows. *Int. J. Refrig.* **2022**, *140*, 57–69. [[CrossRef](#)]
29. Parahovnik, A.; Peles, Y. High pressure saturated flow boiling of CO<sub>2</sub> at the micro scale. *Int. J. Heat Mass Transf.* **2022**, *186*, 122449. [[CrossRef](#)]
30. Lemmon, E.; Huber, M.; McLinden, M. *Standard Reference Database 23: Reference Fluid Thermodynamic and Transport Properties-REFPROP, version 10.0*; National Institute of Standards and Technology, Standard Reference Data Program: Gaithersburg, MD, USA, 2018.
31. Fernando, P.; Palm, B.; Ameel, T.; Lundqvist, P.; Granryd, E. A minichannel aluminium tube heat exchanger—Part II: Evaporator performance with propane. *Int. J. Ref.* **2008**, *31*, 681–695. [[CrossRef](#)]
32. Gungor, K.E.; Winterton, R.H.S. A general correlation for flow boiling in tubes and annuli. *Int. J. Heat Mass Transf.* **1986**, *29*, 351–358. [[CrossRef](#)]
33. Cooper, M.K. Saturated nucleate pool boiling: A simple correlation. *1st UK Natl. Heat Transf. Conf.* **1984**, *2*, 785–793.
34. Thome, J.R. Wolverine Engineering Data Book III, Chapter 10. In *Boiling Heat Transfer Inside Plain Tubes*; 2010. Available online: [https://www.academia.edu/7861284/Engineering\\_Data\\_Book\\_III\\_Boiling\\_Heat\\_Transfer\\_Inside\\_Plain\\_Tubes\\_10\\_1\\_Boiling\\_Heat\\_Transfer\\_Inside\\_Plain\\_Tubes](https://www.academia.edu/7861284/Engineering_Data_Book_III_Boiling_Heat_Transfer_Inside_Plain_Tubes_10_1_Boiling_Heat_Transfer_Inside_Plain_Tubes) (accessed on 7 September 2022).